Reverse-twisting of helicoidal shells to obtain neutrally stable linkage mechanisms

Radaelli, Giuseppe

DOI
10.1016/j.ijmecsci.2021.106532

Publication date
2021

Document Version
Final published version

Published in
International Journal of Mechanical Sciences

International Journal of Mechanical Sciences 202–203 (2021) 106532

Contents lists available at ScienceDirect

International Journal of Mechanical Sciences

journal homepage: www.elsevier.com/locate/ijmecsci

Reverse-twisting of helicoidal shells to obtain neutrally stable linkage mechanisms

Giuseppe Radaelli [a]

Department Precision and Microsystems Engineering, Delft University of Technology, Mekelweg 2, Delft, 2628 CD, The Netherlands

ARTICLE INFO

Keywords:
Helicoidal shells
Neutral stability
Multi-stability
Compliant joints
Compliant mechanisms

ABSTRACT

Mechanisms that consist of many elements and are potentially small sized, benefit from kinematic elementary units like revolute joints that are compliant and monolithic, and therefore could be produced without need for assembly. We present a novel concept of a compliant revolute joint that features low axis drift, high support stiffness and a large range of motion. The concept is based on a helicoidal shell of which a portion reverses its twist direction upon application of a rotation. The reversed region increases gradually, resulting in a constant reaction moment. Analytical, numerical, and experimental analyses are presented to reveal and quantify the constant-moment behaviour. Prototypes of the concept are employed in exemplary linkages to demonstrate the ability to create a large variety of neutrally stable compliant linkages, which require extremely low actuation forces and exhibit large ranges of motion.

1. Introduction

With the desire to create mechanical devices that are ever smaller and cheaper, engineers have been working on so-called compliant mechanisms for the past couple of decades[1]. Mechanisms of this type, namely, gain their mobility from the flexibility of their segments and have the potential to be manufactured as monolithic wholes, and are thus potentially suitable for miniaturization. The fundamentals of compliant mechanism design are being applied to adjoining research branches like metamaterials (a.k.a. architected materials) [2,3], origami mechanisms [4,5], soft-robotics [6,7], and Micro Electronic Mechanical Systems (MEMS) [8,9]. In many cases, compliant mechanisms have been designed as wholes, for specific functionalities. A commonly used technique for this purpose is, e.g., topology optimization [10–12]. In many other cases, however, research has been directed towards designing units with specific yet generally applicable behaviour, useful for integration into modular designs. Examples are constant force and moment generators [13,14], bi-stable units [15–18], linear motion guides [19,20], and, probably the most applicable in modular designs, revolute joints[21].

Revolute joints are the quintessential element of mechanisms with a kinematic goal, i.e. to realise a certain motion and constrain all others. Therefore, a significant part of the investigations on compliant mechanisms has been directed towards realising revolute joints [21–25] that mimic as much as possible the behaviour of classical joints, and that take advantage of the typical strengths of compliant mechanism: the absence of friction, play, wear, needed assembly and needed lubrication [26]. The availability of such units would make it possible to apply the well-established paradigms in classical mechanism design to the design of compliant mechanisms. This becomes especially relevant for designs consisting of many elements, like (robotic)metamaterials, deployable structures, and reconfigurable mechanism, who can be especially jeopardized by compliance in the constrained directions and stiffness in the motion direction, intrinsic to most compliant mechanisms.

Mimicking the ideal kinematic behaviour with compliant mechanisms involves multiple challenges. Trease et al. [23] suggested five main criteria to evaluate the performance of compliant revolute joints, namely the range of motion, axis drift, ratio of off-axis stiffness to stiffness about the axis of rotation, stress concentrations, and compactness. Many designs of compliant joints have been focussing on minimizing the axis drift, and maximizing the support stiffness and the range of motion.

The well-established concept of the notch-type joints was first described by Paros [27], then further optimized by Linß [28,29]. This class of joints is often favoured in precision applications, where very limited ranges of motion suffice. Also the cross-spring pivot has been described, modelled, applied and optimized extensively for a long time now [30–36]. This concept significantly increases the range of motion with respect to the notch-type joints, not being as critical for stress concentrations. However, the range of motion is still bounded by the eventual self-intersection of the two extremes of the joint. Moreover, cross-spring pivots generally suffer from axis drift. On a similar note, the butterfly joint [37], the infinity joint [22], and similar joints that are essentially based on planar bending deformation, are successfully

E-mail address: g.radaelli@tudelft.nl

https://doi.org/10.1016/j.ijmecsci.2021.106532
Received 1 March 2021; Received in revised form 11 May 2021; Accepted 11 May 2021
Available online 24 May 2021

improved in terms of support stiffness and axis drift, but are limited in the range of motion by self-intersection.

On the other hand there are concepts that are based on an internal shaft and an external rim connected by multiple radially arranged flexural members [38,39]. Variations to this concept have been proposed with so-called contact-aided flexures [40], which improve the support stiffness. However, in general, when one of the performance criteria is optimized, it goes to the expense of another. A comprehensive overview of compliant joints that includes also most of the work cited above is given by Farhadi [21].

It is noticeable from the overview that most concepts are based on planar flexures, and, as a consequence, the range of motion is eventually limited because of self-intersection. The two exceptions are those that are based on torsion, and thus have an intrinsically spatial character: the CR joint [23] and the split-tube [41]. These joints are able to reach an exceptional compromise between torsional compliance, off-axis stiffness, axis drift and range of motion. The concepts consist of torsionally loaded extrusions of a cruciform cross-section and an open circle, respectively. Due to the open nature of these cross-sections, a relatively low torsion stiffness is achieved while the bending stiffness is maintained high. This distinctive result encourages the investigation into compliant joints with an inherently spatial working principle.

Instead of increasing the support stiffness, other authors have focussed their efforts towards eliminating the rotational stiffness of joints by applying static balancing techniques, thereby making it a matter of relative stiffness ratios. Indeed, in a relative sense, a zero rotational stiffness about the axis of rotation makes all other off-axis stiffnesses infinite. Work on statically balanced compliant mechanisms (SBCM) [42] also goes by the names of neutrally stable structures or zero-stiffness structures [43]. The fundamental idea of these approaches is to introduce energy trough prestress in a structure and make sure that if a part of the structure deforms absorbing elastic energy, another part provides the same amount of energy by un-deforming. For this to happen, it is often convenient to design compliant parts with certain specifically required nonlinearity. In a broader context, also others have managed to design joints with integrated spring functionality, e.g. [44], both linear and nonlinear, by taking advantage of the inherent presence of rotational stiffness in compliant mechanisms.

From the work on statically balanced compliant joints, two classes of planar solutions can be distinguished, equivalent to the distinction made above for the non-balanced solutions. In the first class, applied by Morsch [34], Zhao [45] and Merriam [46], the concept is used where pretensioned flexures on the side of a cross-axis flexural pivot eliminate its rotational stiffness. The second class of solutions involves the use of radially arranged curved flexures connecting an outer rim to an inner shaft. The shape of the flexures can be manipulated in such a way that the resulting moment-angle characteristic becomes constant [14,47–49]. In theory, two constant moment units can be arranged in opposite sense to obtain a zero-moment behaviour. In this class of solutions, however, the coaxiality of the rim and the shaft cannot be guaranteed by the compliant members themselves but has to be imposed by an additional constraint, like a bearing. This limitation impedes the use of these designs as independent revolute joints.

A spatial class of solutions used to obtain zero torsional stiffness is developed by Lachenal [50] in his effort to develop shape-morphing aircraft wings. The concept is based on an I-beam with two precurved flanges bonded to a straight web. The flanges provide a negative stiffness component that neutralizes the positive stiffness of the whole structure. Another example of a spatial solution is proposed by Li [51]. The complex spatial deformation of radially arranged strips produces a nonlinear moment-angle characteristic that under certain circumstances approximates a constant moment. However, also in this example, an additional support must be provided to maintain coaxiality of the input and output shaft, making them inadequate as independent revolute joints. It is the combination of torsion-based solutions with stiffness reduction techniques that appears to be the most promising strategy for upcoming developments.

In this paper we present a new compliant rotational joint concept based on a helicoid-shaped shell, featuring exceptional kinematic performances. Due to its spatial working principle, self-intersection is avoided, thus yielding very large ranges of motion. Furthermore, it exhibits a high off-axis stiffness, and an axis drift that can go as low as zero, depending on the loading condition. Peculiarly, the presented design exhibits an inherent constant moment upon an applied rotation. This constant moment can be neutralized by an equal, opposing constant moment, resulting in a neutrally stable joint, i.e. one where the elastic forces do not counteract the intended motion. It is also shown that the constant-moment joint can potentially be used to render any linkage neutrally stable, tremendously benefiting their efficiency. The concept can easily be extended to include other type of intentional spring behaviour, such as multi-stability and other non-linearities.

In the following, we first introduce the general concept of a helicoidal shape which locally reverses its twist upon an imposed rotation, substantiated by a theoretical model based on inextensible shell theory. Then we analyse the moment-angle profile of the joints with a variety of design parameters by using a finite element model as well as by experiments. Further on, the support stiffness and axis drift are assessed numerically and experimentally, by introducing a novel dimensionless kinematic measure. To conclude, we show the application of the developed joints in a number of classical linkage mechanisms, demonstrating the ability to generate neutrally stable mechanisms with both open and closed kinematic chains.

2. Method and results

In coming subsections, the working principle is first described qualitatively and then substantiated with the theoretical developments, numerical analyses and experiments performed on the helicoidal compliant revolute joint.

2.1. Working principle

The working principle of the presented compliant revolute joint (Fig. 1, see Supplementary Video 1) is based on the reverse twisting of a helicoidal shell. We consider a shell structure consisting of at least three one-sided right helicoidal shells joined along their common edge in the middle. Following the assumptions of inextensible shells, which require the preservation of Gaussian curvature upon deformation of a thin shell, we observed that a full reversion of the twist direction of the helicoids results in a shape with unchanged Gaussian curvature. Thus the undeformed helicoid and the helicoid with reversed twist are isometric, i.e. the lengths on the mid-surface of the shell do not change upon deformation. It follows that the fully reversed state is energetically convenient with respect to other deformations which would require stretching or compression of the mid-surface.

A remarkable behaviour emerges when the reversion of the twist is applied gradually. As a relative rotation is applied between the two ends of the joint, there is a portion of the helicoid that snaps into a reverse-twist state because of the low deformation energy of that mode, while the rest of the helicoid remains practically undeformed. Two peculiar phenomena emerge from this state of deformation. The first one is that the length of the reverse-twist region is proportional to the applied rotation angle. It follows that the elastic energy increases linearly with the applied rotation angle. By the definition of generalized conservative forces, the reaction moment corresponding to the applied rotation is then constant, and the rotational stiffness equals zero. The condition of constant moment and zero stiffness holds until the whole joint is reversed. The second remarkable phenomenon is that if the rotation angle is kept constant, the reverse-twist region can be moved up and down the geometry without affecting its length. That implies that the total stored

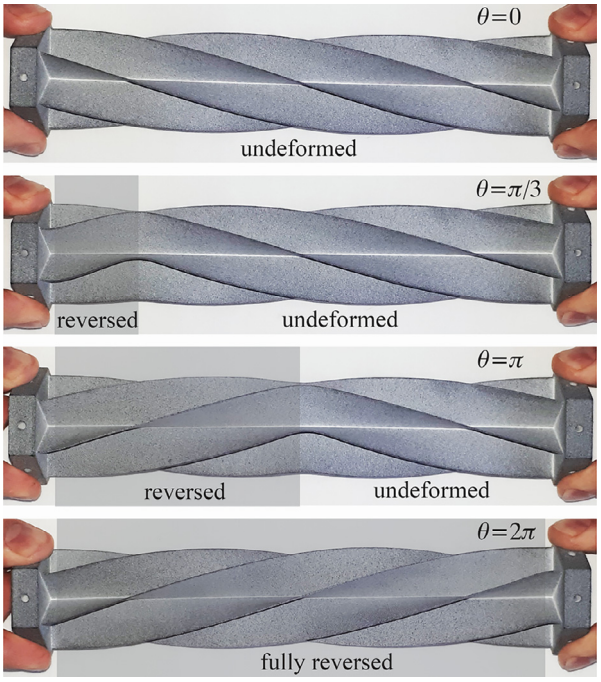

Fig. 1. By imposing a rotation between the two extremities, a helicoidal shell joint exhibits a reversal of the twist that is bound within a distinct region. The rest of the joint remains practically undeformed. The region of reversed twist increases proportionally to the applied angle until the helicoid is fully reversed. Assuming that the strain energy is significant only in the reversed region, it can be deduced that the strain energy increases proportionally to the applied angle, and consequently, the applied moment is constant. See Supplementary Video 1.

energy remains constant and that every position of the reverse-twist region yields static equilibrium: it is neutrally stable. The reversed-twist region can also be moved up and down by rotating it about the middle-axis, yielding, in essence, a zero-moment rotational joint. It must be noted that the described behaviours only appear when the angle applied between the ends of the joint are in the opposite direction of twist, considering that turning in the same direction of the twist would essentially merely stretch the helicoids, thus yielding a high torsional stiffness.

2.2. Theory and characterisation

To derive the equations that relate an applied rotation to the resulting reaction moment, at first we consider a helicoidal shell that gets fully reversed. The mid-surface of a one-sided right helicoidal shell can be described parametrically in Cartesian coordinates as

$$S(u,v) = (u\cos(\alpha v), u\sin(\alpha v), v), \tag{1}$$

where the parameters u and v are defined within the intervals $[0, w]$ and $[0, h]$ respectively, with w and h the width and height of the helicoid, see Fig. 3a, and where α is the rate of angle of twist, defined as

$$\alpha = \frac{d\phi}{dv} = \frac{\Phi}{h}, \tag{2}$$

where ϕ is the angle of twist, and Φ is the angle of twist at $v = h$. Similarly, a fully reversed helicoid can be described by eq. (1), replacing the rate of angle of twist by its negative value $-\alpha$. To twist the undeformed helicoid into the fully reversed helicoid a relative rotation θ between the bottom and top must be applied, equal to

$$\theta_{max} = 2\Phi. \tag{3}$$

This is likewise the maximum range of motion of the joint.

Calladine's definition of the strain energy of bending per unit area of a shell [52] is given by

$$U_B = \frac{1}{2}D\Big[(\kappa_x + \kappa_y)^2 + 2(1-\nu)(-\kappa_x\kappa_y + \kappa_{xy}^2)\Big], \tag{4}$$

where D is the flexural rigidity, ν is Poisson's ratio, and κ_x, κ_y, and κ_{xy} are the curvature changes in the perpendicular directions x and y, and the change in twist curvature, respectively. The flexural rigidity is defined by

$$D = \frac{Et^3}{12(1-\nu^2)}, \tag{5}$$

with E, the Young's modulus, and t, the thickness of the shell. The condition of inextensibility and the compatibility with the constrain that holds the inner edge on the middle-axis, result in a simplification of eq. (4) that only accounts for energy contribution by the change in twist curvature, thus yielding

$$U_B = \frac{1}{2}D\Big[2(1-\nu)\kappa_{xy}^2\Big]. \tag{6}$$

Since the twist curvature changes from undeformed to fully reversed, the change in twist curvature equals

$$\kappa_{xy} = 2\alpha. \tag{7}$$

The total strain energy in a fully reversed helicoid is obtained by integrating eq. (6) over the area A of the helicoidal shell, as

$$U_{full} = \int\int_A \frac{1}{2}D\Big[2(1-\nu)\kappa_{xy}^2\Big]dA, \tag{8}$$

where thee infinitesimal area dA is given in parametric form as

$$dA(u,v) = \sqrt{\alpha^2u^2+1}\,dudv. \tag{9}$$

In a helicoid that is only partially reversed, three types of regions can be distinguished: a fully reversed region, one or more non-reversed regions, and transition zones there in-between. In the transition zones the shell is not able to simultaneously fulfil the inextensibility condition and the edge constrain. The strain energy in the transition zones can thus not be derived from eq. (4). Advantageously, the shape of the transition zones are observed to be unchanging during the process of reversing the twist of the helicoid. Therefore, its contribution to the strain energy can be considered as an unknown constant term. The influence of this approximation is assessed by the numerical simulation described in Section 2.3. When a relative rotation θ is applied between the top and the bottom of the helicoid, the reversed part increases in length at the expense of the undeformed region. The relative angle between the upper and lower edges of the helicoid equals the integral of the rate of angle of twist over the height

$$\Phi - \theta = \int_0^h \alpha(v)dv. \tag{10}$$

Considering that the rate angle of twist α is constant for both the unreversed and the reversed regions, only opposite in sign, it follows that the length of the reversed region increases linearly with the applied angle θ. This makes it possible to derive the reaction moment corresponding to an applied rotation as the derivative of the strain energy with respect to the applied angle, as a ratio of the strain energy of the fully reversed helicoid over the maximum applied rotation, thus yielding

$$M_z = \frac{U_{full}}{\theta_{max}}N, \tag{11}$$

where the multiplier N is the number of helicoids that constitute the entire joint.

Interestingly, for a given applied angle θ, the integral of eq. (10) can be satisfied in an infinite number of ways by sliding the region of reversed twist along the height, without affecting the total energy, eq. (8), which proves that this mode of deformation is neutrally stable.

2.3. Numerical and experimental analysis

The equations derived in Section 2.2 model the general behaviour of a helicoidal joint. This model includes the reverse-twisted region of the helicoid and assumes that only the twist deformation contributes

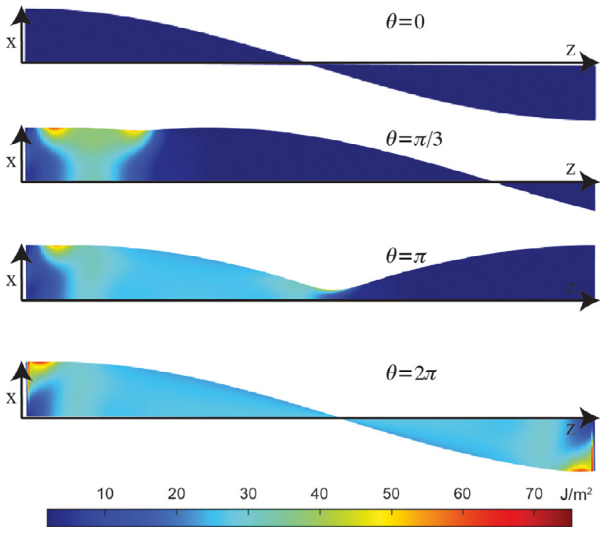

Fig. 2. Strain energy density distribution of a helicoidal shell upon advancing twist reversal. In the reversed region, the strain energy density is uniform to a large extent, and does not change with the applied rotation. At the edges of this region, the energy density has a peak. Even these peaks, however, are not affected by the applied rotation, except for the locations at which they appear. See Supplementary Video 2.

to the total energy. However, it excludes the transition zones where a more complex deformation occurs, including bending and membrane deformations. The transition zones are formed during an initial snap-through caused by the applied rotation. After that, the transition zones stabilize and do not constitute a substantial change in the total elastic energy of the system. To comprehend the effects taking place in the transition zones, an analysis is performed using a finite element model of a Kirchhoff-Love shell with a linear elastic constitutive law. This model captures bending as well as membrane deformations. For the material, a Young's modulus of 1.8GPa and a Poisson's ratio of 0.38 was used, corresponding to Nylon (PA12) which is used for the prototypes.

The constraints and loading conditions as implemented in the finite element analysis are illustrated in Fig. 3(b). Fig. 2 shows the elastic energy density distribution on the deformed shell, matching the applied rotation of Fig. 1. Fig. 4 shows the progression of the energy density as a rotation θ is applied to the joint. In both figures it can be noticed that the energy redistributes over an increasing region of the helicoid, the reversed region, while the magnitude of the energy density stays approximately constant. It can also be observed that the energy contribution of the transition zones barely changes as they travel along the height of the structure.

The influence of the geometrical design parameters, namely the thickness t, the width w, the rate of angle of twist α and the height h, was analysed. For that purpose the geometry of a *standard design* is defined with $t = t_0 = 0.4 \times 10^{-3} m$, $w = w_0 = 0.1^{-1} m$, $\alpha = \alpha_0 = \frac{\pi}{0.1}\text{radm}^{-1}$, and $h = h_0 = 0.1\text{m}$. The parameters t, w and α are varied in the range from half to twice the value of the *standard design*. In order to obtain a comparable range of motion for all analysed geometries, the total twist angle is kept constant to $\Phi = \pi$. It follows that the height parameter h depends on α, according to Eq. (2). The moment corresponding to an applied rotation is shown for the mentioned variations in Fig. 5a-c. The dashed lines represent the analytical result and the solid lines are obtained from the finite element analysis.

The moment-rotation response was also determined experimentally on a torque-test-bench, with prototypes obtained by additive manufacturing (HP Multi Jet Fusion), consisting of six helicoids merged at the central axis. The material used for all prototypes is Nylon, type PA12. The experimental results are shown and compared to the analytical model in Fig. 5(d-f). The analyses show agreement on the influence of

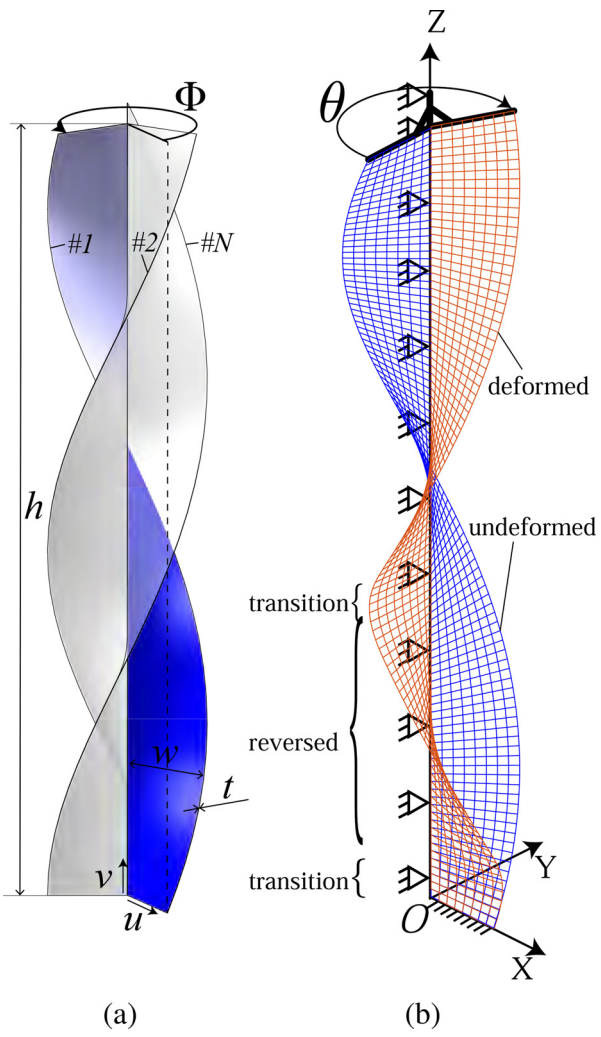

Fig. 3. a) The compliant revolute joint is described by the geometric parameters of a one-sided right helicoidal shell (the thickness t,the width w, the height h, and the angle of twist Φ), and the number of helicoids N that form the joint. b) The finite element model is shown in undeformed (blue) and deformed (red) state. The translational degrees of freedom of the nodes at the middle edge are all constrained. A clamping constrain is applied on the lower edge, and a rotating clamping constrain is applied on the upper edge, where the rotation θ is applied. (For interpretation of the references to colour in this figure legend, the reader is referred to the web version of this article.)

the parameters, namely that the thickness has cubic influence on the moment, while the influence of the width and the rate of angle of twist is linear. The height of the joint has no influence on the value of the constant moment, but increases the range of motion linearly, in accordance with eq. (3) and eq. (2). The analytical model gives a valid initial estimate of the constant moment. The numerical simulation also shows the progression of the moment, especially in the beginning and at the end of the range of motion, and also, it shows a slight monotonic increase within the presumed constant moment range. This component is supposedly related to the regular (Saint-Venant) torsional stiffness of the joint, caused by shear deformation, which is disregarded in the analytical model.

2.4. Support stiffness and axis drift

Because of the rotational symmetry of the structure, when a pure moment is applied, the axis drift is zero. However, a joint is also expected to resist other loads without substantially alter its kinematics. Therefore, for the employment of the helicoidal shell concept as a revo-

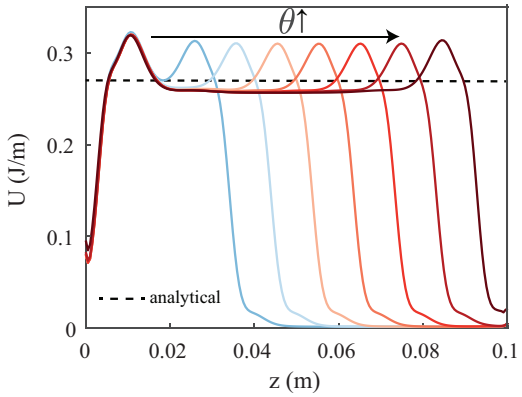

Fig. 4. The graph shows the strain energy density of a helicoidal shell as a function of the vertical coordinate z, for an increasing applied rotation θ. Once a part of the shape snaps into a reversed twist state, the strain energy density distribution does not increase in magnitude, but only widens its window. The data from the finite element simulation (solid lines) is compared to the value obtained by the analytical approximation (dashed line) in this graph.

lute joint solution, it is necessary to relate the torsional moment to the bending stiffness that keeps the revolute joint centered to the middle axis. For that purpose, the 6x6 linear compliance matrix, i.e. the inverse of the stiffness matrix, related to the endpoint of the joint is given for the standard design as

$$\begin{pmatrix} \frac{\partial(\boldsymbol{u}_{xyz})}{\partial(\boldsymbol{F}_{xyz})} & \frac{\partial(\boldsymbol{\theta}_{xyz})}{\partial(\boldsymbol{F}_{xyz})} \\ \frac{\partial(\boldsymbol{u}_{xyz})}{\partial(\boldsymbol{M}_{xyz})} & \frac{\partial(\boldsymbol{\theta}_{xyz})}{\partial(\boldsymbol{M}_{xyz})} \end{pmatrix}$$

$$= \left(\begin{array}{ccc|ccc} 0.0011 & 0.0000 & 0.0000 & 0.0040 & 0.0146 & 0.0000 \\ . & 0.0011 & 0.0000 & 0.0146 & 0.0040 & 0.0001 \\ . & . & 0.0000 & 0.0000 & 0.0000 & 0.0027 \\ \hline . & . & . & 0.3053 & 0.0008 & 0.0046 \\ . & . & . & . & 0.3722 & 0.0002 \\ . & . & . & . & . & 3.0041/\infty \end{array}\right)$$

Herein the compliance value for the torsional stiffness $c_{\theta_z} = \frac{\partial \theta_z}{\partial M_z}$ is given for the undeformed configuration as well as for the constant-moment range, yielding an infinite compliance. All other compliance values are determined at the undeformed configuration. The lower-left part of the matrix is left empty because of symmetry.

To analyse how well the joint resists lateral forces in a more concise fashion, and to be able to compare the effect of each design parameter, a novel performance criterion is introduced. There are two important circumstances that make such a criterion necessary. First, because the joint exhibits a constant torsional moment, thus a zero torsional stiffness, in comparison the lateral stiffness will always appear infinitely high. Secondly, the constant moment will in most cases not be a pure moment but will result from an unbalanced lateral force times a distance. It means that there is an implicit relation between the constant

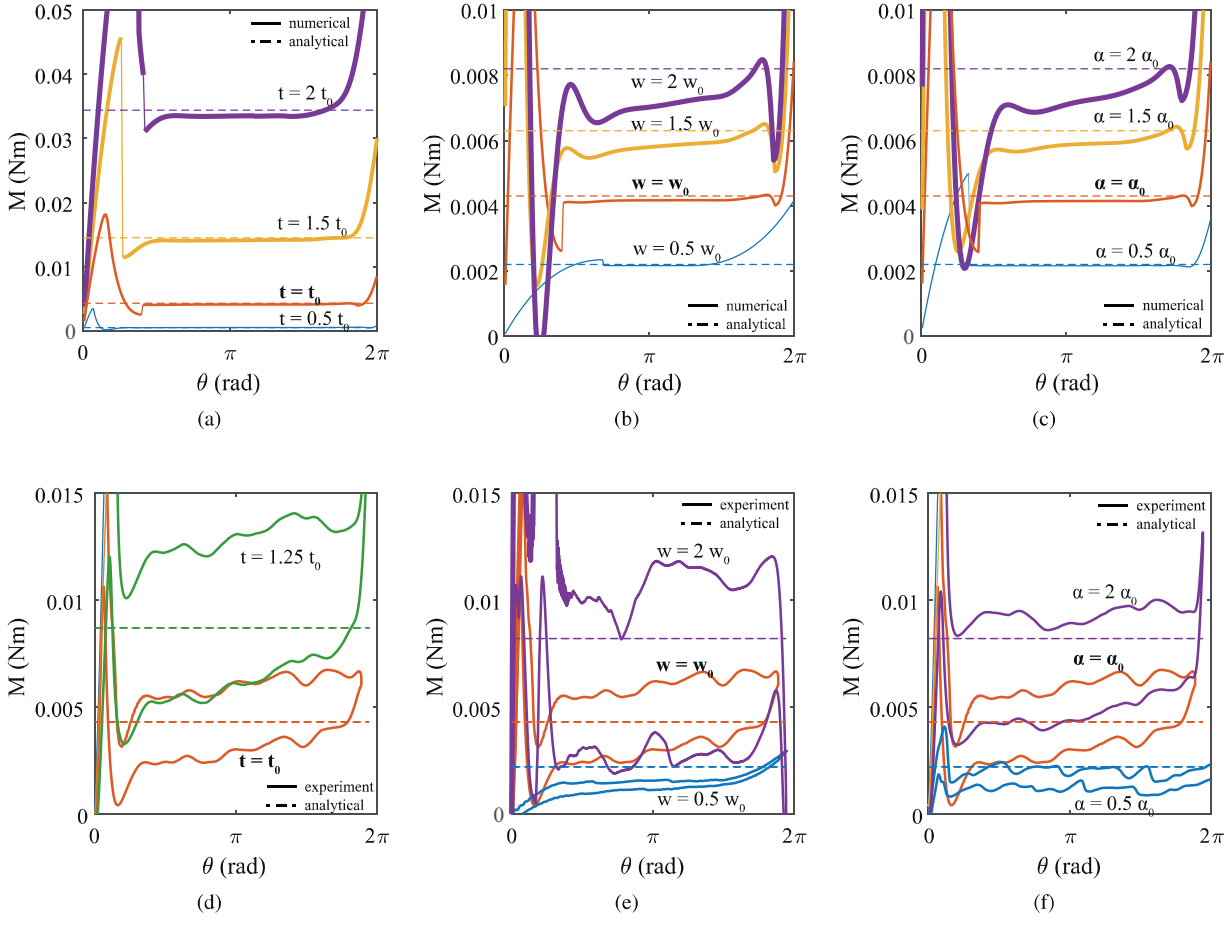

Fig. 5. The constant moment values obtained analytically for a variety of geometrical design parameters is compared with the simulated results (a-c) and to the experimental results (d-f). a) and d) show the variation of the shell-thickness, ranging from $0.5t_0$ to $2t_0$ with $t_0 = 0.4 \times 10^{-3} m$. The thickness range of the experimental results is more limited because of strength limitations of the applied material and production method. b) and e) show the variation of the shell width, ranging from $0.5w_0$ to $2w_0$ with $w_0 = 0.1 \times 10^{-1} m$. c) and f) show the variation of the rate of angle of twist, ranging from $0.5\alpha_0$ to $2\alpha_0$ with $\alpha_0 = \frac{\pi}{0.1}\text{radm}^{-1}$.

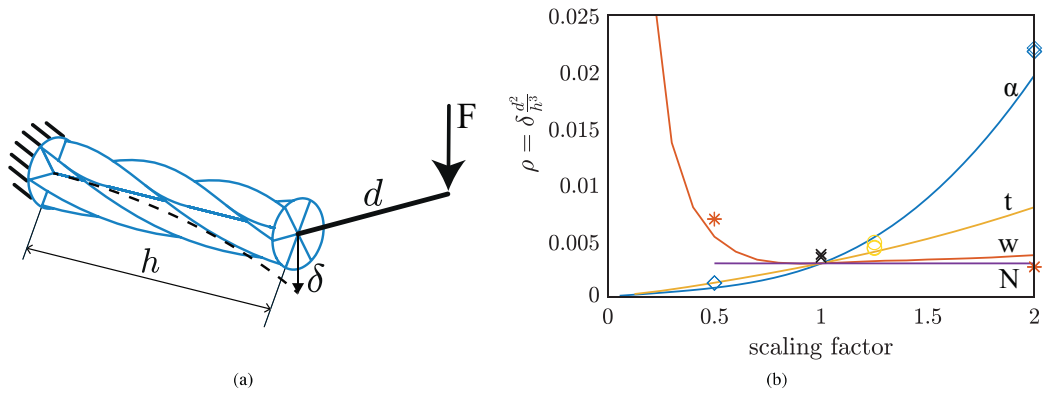

Fig. 6. The non-dimensionalised form of the lateral deflection δ is plotted for the variations of the design parameters t, w, α and N. The scaling factor parameter on the horizontal axis is defined as a multiplication with respect to the design parameter of interest in the *standard design*, namely t_0, w_0, α_0 and $N = 6$. The data represented by the solid lines is obtained by a finite element analysis of the helicoidal joints in a cantilever type loading condition. The scattered data points are obtained from experiments with equivalent loading conditions ($\circ = t$, $* = w$, $\Diamond = \alpha$, $\times =$ *standard design*, N is not varied in experiments).

moment and the lateral force. Therefore, only looking at the stiffness or compliance values does not give sufficient insight.

The presented criterion relates the complex elastokinematic behaviour of a compliant joint to a purely kinematic measure. This is done by assuming that in a practical embodiment of the joint, the torsional moment is applied by a single sided force F at a moment arm d, as shown in Fig. 6a. In practice, this moment arm d would be of the same order of magnitude as the length of the links connected by the joint within a linkage chain. From the torsional moment M_z, which is approximately constant, the force F can be determined for every set of design parameters and a chosen moment arm d. In a cantilever-type clamping condition, the force F does not only yield the desired twist deformation, but also results in a lateral deflection δ. This deflection reflects an undesired offset of the center of rotation, also called axis drift. A non-dimensionalised form of the lateral deflection δ is proposed, defined as

$$\rho = \delta \frac{d^2}{h^3}. \tag{12}$$

This non-dimensionalised form permits to present the remainder of the bending analysis in a more general way, not relying on specific choices related to the height h and the moment arm d, which may vary substantially for different applications of the compliant joint. The height h, in fact, has cubic influence on the deflection δ, similar to the effect of the length of a beam in a cantilever loading condition. The effect of the moment arm d on the other hand is inversely proportional: The same torsional moment M_z can be applied by a smaller lateral force F if the moment arm d increases. In addition, the lateral deflection δ is normalised by the moment arm d to yield a relative lateral deflection $\hat{\delta} = \delta/d$. This measure is taken because the axis drift of a joint is usually not relevant in absolute sense, but only in relation to the size of the linkage chain where the joint is embedded. For the standard design, the criterion yields a value of $\rho = 3.0e-3$, meaning that choosing, e.g., $h = d = 0.1$m, gives the deflection $\delta = 3.0 times 10^{-4}$m. Normalised by the moment arm d, it yields a relative lateral deflection of $\hat{\delta} = 3.0 \times 10^{-3}$, or 0.3%.

A parameter-influence study on the lateral deflection criterion is shown in Fig. 6b. The criterion is calculated using a linear finite-element analysis of a joint composed of $N = 6$ non-reversed helicoids. The simulated joints were clamped at their basis, loaded by a lateral force F on the opposite end, without a moment arm, i.e. $d = 0$. From the constant moment M_z obtained from the analytical model for every set of design parameters, the lateral force F can be paired to a chosen value of the moment arm d. Thus, from the simulated lateral force-deflection data, the lateral deflection δ is determined for a chosen finite moment arm d. This is the lateral deflection that the joint would exhibit if a rotation was applied to the joint by turning a link with length d. The non-dimensionalised criterion ρ obtained from the lateral force deflection simulations, is shown in Fig. 6. Every line represents the variation of a design parameter, expressed as a scaling factor with respect to the value in the standard design. It is remarkable to note from the results of the finite element analysis, that the influence of the number of helicoids N of a joint does not seem to affect the axis drift. In fact, a higher number N of helicoids in a joint increases the required constant moment M_z by the same factor as it increases its bending stiffness.

The data in Fig. 6 is validated experimentally by force-deflection experiments on the non-reversed geometries. In concordance with the simulation, the prototypes were clamped at their basis and loaded with an imposed lateral deflection at the other end, while the reaction force was measured. The non-dimensionalised criterion ρ, obtained from the lateral force-deflection experiments on the same set of prototypes as the torsional experiments, is shown in the figure by coloured markers, where the colours correspond to the line colours of the simulated data.

3. Integration: neutrally stable linkages

With the goal to generate neutrally stable linkage mechanisms, two cases are distinguished: linkages with a closed loop, and linkages with an open loop. In the case of linkages with closed loops, e.g., parallelogram mechanisms, four-bar mechanisms, and linkages with scissor-pairs, the constant-moment joints can be employed directly. For every closed loop the sum of interior angles remains constant upon deformation. Therefore, the potential energy of the whole system remains constant for all deformations, even for systems with more than one degree of freedom, provided that each joint remains within its constant-moment range. It is necessary to preload the system in order to bring it in a configuration that satisfies the latter requirement. Rotating the joint in the opposite direction, or beyond the constant moment region would disturb the neutral stability because of the steep increase of the torsional moment that would result from it. We have created a neutrally stable four-bar linkage and a neutrally stable six-bar linkage according to this principle. Pictures of the moving mechanisms are shown in Fig. 7 and Fig. 8 (see Supplementary Video 3 and Supplementary Video 4). The lengths of the links in the shown mechanisms are arbitrary, since any combination of lengths would satisfy the neutral stability condition.

Even neutrally stable open chains can be generated, provided that the joints are used in their zero-moment modus. That means that the reversion of the twist is initiated, and that the reversed region is used as output of the joint. Equivalently, it is possible to stack two joints in a collinear fashion and initiate the reversion by applying a rotation to the two extremes. Then, the connection of the joints can be used as the output of the assembled joint. Using this technique with two pairs of helicoidal joints, we have created a two-link open chain that is neutrally

Fig. 7. A neutrally stable four-bar linkage (orange schematic) is constructed with rigid links (black) and helicoidal shell joints (grey). The joints are preloaded such that they act in their constant moment range. At the bottom, top-views of a number of equilibrium positions are shown. See Supplementary Video 3.

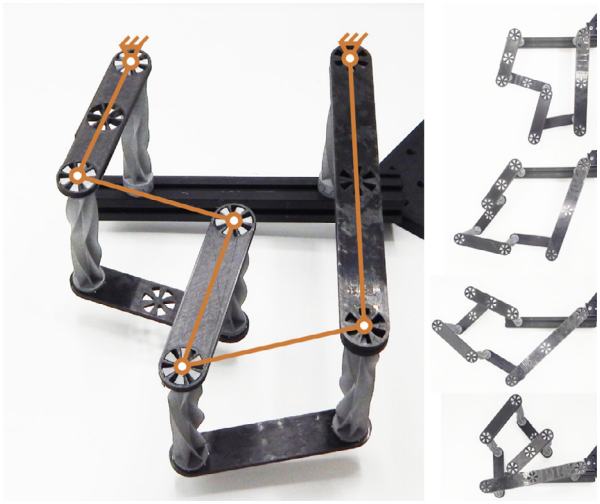

Fig. 8. A neutrally stable six-bar linkage (orange schematic) is constructed with rigid links (black) and helicoidal shell joints (grey). The joints are preloaded such that they act in their constant moment range. On the side, top-views of a number of equilibrium positions are shown. See Supplementary Video 4.

stable throughout a very large range of motion for all two degrees of freedom. The motion of the linkage is illustrated in Fig. 9 (see Supplementary Video 5).

4. Discussion and conclusion

A novel monolithic compliant revolute joint which features a constant moment, a large range of rotational motion, high support stiffness and small axis drift is presented. The joint consists of a composition of helicoidally shaped shells. Upon application of a rotation, the helicoids progressively reverse to the opposite direction of twist. The joints can easily be integrated into linkage-type mechanisms, and the constant moment enables the possibility to generate neutrally stable linkages. Mechanisms consisting of many linkages and joints, like deployable structures and metamaterials, are limited in their behaviour by the absorption of strain energy by the elements of the mechanism and by poor kinematic

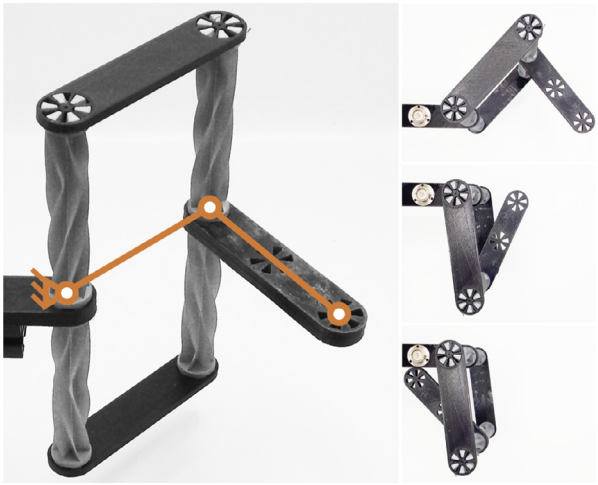

Fig. 9. A neutrally stable two-link open chain (orange schematic) is constructed with rigid links (black) and helicoidal shell joints (grey). Here, the helicoidal joints are used in collinear, preloaded pairs. In the range where both joints in a pair produce a constant but opposing moment, the moments cancel out, yielding neutral stability for every joint of the linkage. On the sides, top-views of a number of equilibrium positions are shown. See Supplementary Video 5.

performance due to axis-drift. It is expected that the introduced helicoidal joint will considerably advance the development of such compliant mechanisms with complex topologies.

We introduced an analytical model of the helicoidal joint based on inextensibility conditions of the shell, which is able to predict the magnitude of the constant moment. The model is suitable as an aid to the early design stage of the helicoidal joint.

With a numerical analysis the behaviour of the joint was characterized in its full range of motion, including the effect of the transition zones that were excluded from the analytical model, and thereby, validating it. Both the analytical and the numerical model were used for a parameter study that shows the influence of the thickness, the width, the height and the rate of angle of twist on the behaviour of the joint. Experiments with a torsion bench confirm the predictive ability of the analytical and numerical model, although manufacturing inaccuracies and the presence of visco-elastic losses in the specific material that was used cause significant levels of noise in the experimental data.

In an additional numerical and experimental investigation, the joints were loaded as a cantilevered beam in order to provide a measure for the axis drift under influence of transversal forces. A novel criterion is introduced that captures the complex elastokinematic behaviour into a purely kinematic measure. This is necessary because the matters of support stiffness and on-axis stiffness cannot be seen independently, but on the other hand, when the on-axis stiffness is zero or close to zero, a simple ratio of stiffnesses is not informative since it reduces to zero irrespectively of the support stiffness. The introduced criterion is calculated for the same variation of design parameters as for the constant-moment analysis. Remarkably, according to this criterion, the number of helicoids that form the joint does not affect the lateral deflection. It must be noted that the lateral deflection data, both simulated and experimental, was obtained for joints in the non-reversed state. It is likely that this represents an underestimation of the lateral deflection. Investigating how the progressive reversion of the twist influences the lateral deflection of the joints is a topic of forthcoming research.

The height of the helicoidal joint is highly influential to two main performance indicators of a joint. When leaving all other parameters unchanged, the height relates linearly to the range of motion of constant moment, i.e. a higher joint can produce a constant moment over a larger angle. On the other hand a higher joint results in a decreased lateral stiffness. It is thus important to consider this trade-off when applying the joint, depending primarily on the required range of motion.

Representative embeddings of the helicoidal joints have been fabricated: a four-bar linkage, a six-bar linkage, and a two-link open chain. The prototypes demonstrate the ability to generate complex linkages with neutral stability using helicoidal joints.

The principle of progressive reversion of a helicoidal shell can be generalised to achieve different mechanical behaviour, such as multistability, negative torsional stiffness, and generally, any desired load profile. Of even greater significance would be to obtain single joints that exhibit a range of zero-moment. This would easy the generation of neutrally stable linkages. Moreover it would eliminate the inherent lateral force associated with a finite constant moment, which causes undesired lateral deflection. In order to generate all kinds of load profiles, forthcoming research could be directed towards tailoring the design parameters in a non-constant fashion along the height of the joint.

Declaration of Competing Interest

The authors declare that the research was conducted in the absence of any commercial or financial relationships that could be construed as a potential conflict of interest.

CRediT authorship contribution statement

Giuseppe Radaelli: Conceptualization, Methodology, Software, Data curation, Writing - original draft, Visualization.

Acknowledgment

This work was supported by the Dutch Research Council (NWO) [P16-05 Shell-Skeletons]. The authors also thank Marco Radaelli and Randy Griekspoor for performing preliminary experiments.

Supplementary material

Supplementary material associated with this article can be found, in the online version, at 10.1016/j.ijmecsci.2021.106532

References

[1] Howell LL, Magleby SP, Olsen BM. Handbook of compliant mechanisms. 1st Edition. New York: John Wiley & sons, inc; 2013.
[2] Shaw LA, Chizari S, Dotson M, Song Y, Hopkins JB. Compliant rolling-contact architected materials for shape reconfigurability. Nat Commun 2018;9(1):1–12. doi:10.1038/s41467-018-07073-5.
[3] Kim K, Heo H, Ju J. A mechanism-based architected material: ahierarchical approach to design poisson's ratio and stiffness. Mech Mater 2018;125(June):14–25. doi:10.1016/j.mechmat.2018.07.001.
[4] Greenberg HC, Gong ML, Magleby SP, Howell LL. Identifying links between origami and compliant mechanisms. Mech Sci 2011;2(2):217–25. doi:10.5194/ms-2-217-2011.
[5] Delimont IL, Magleby SP, Howell LL. Evaluating compliant hinge geometries for origami-inspired mechanisms. J Mech Robot 2015;7(1):1–8. doi:10.1115/1.4029325.
[6] Nurzaman SG, Iida F, Margheri L, Laschi C. Soft robotics on the move: scientific networks, activities, and future challenges. Soft Rob 2014;1(2):154–8. doi:10.1089/soro.2014.0012.
[7] Liu CH, Chen TL, Chiu CH, Hsu MC, Chen Y, Pai TY, et al. Optimal design of a soft robotic gripper for grasping unknown objects. Soft Rob 2018;5(4):452–65. doi:10.1089/soro.2017.0121.
[8] Kota S, Ananthasuresh GK, Crary SB, Wise KD. Design and fabrication of microelectromechanical systems. Journal of Mechanical Design, Transactions of the ASME 1994;116(4):1081–8. doi:10.1115/1.2919490.
[9] Kota S, Joo J, Li Z, Rodgers SM, Sniegowski J. Design of compliant mechanisms: applications to MEMS. Analog Integr Circuits Signal Process 2001;29(1–2):7–15. doi:10.1023/A:1011265810471.
[10] Sigmund O. On the design of compliant mechanisms using topology optimization. Mechanics of Structures and Machines: An International Journal 1997;25(4):493–524. doi:10.1080/08905459708945415.
[11] Bruns TE, Tortorelli DA. Topology optimization of non-linear elastic structures and compliant mechanisms. Comput Methods Appl Mech Eng 2001;190(26–27):3443–59. doi:10.1016/S0045-7825(00)00278-4.
[12] Kirmse S, Campanile LF, Hasse A. Synthesis of compliant mechanisms with selective compliance an advanced procedure. Mech Mach Theory 2021;157:104184. doi:10.1016/j.mechmachtheory.2020.104184.
[13] Wang P, Xu Q. Design and modeling of constant-force mechanisms: asurvey. Mech Mach Theory 2018;119:1–21. doi:10.1016/j.mechmachtheory.2017.08.017.
[14] Gandhi I, Zhou H. Synthesizing constant torque compliant mechanisms using precompressed beams. Journal of Mechanical Design, Transactions of the ASME 2019;141(1). doi:10.1115/1.4041330.
[15] Jensen BD, Howell LL. Bistable configurations of compliant mechanisms modeled using four links and translational joints. Journal of Mechanical Design, Transactions of the ASME 2004;126(4):657–66. doi:10.1115/1.1760776.
[16] Hansen BJ, Carron CJ, Jensen BD, Hawkins AR, Schultz SM. Plastic latching accelerometer based on bistable compliant mechanisms. Smart Mater Struct 2007;16(5):1967–72. doi:10.1088/0964-1726/16/5/055.
[17] Oh YS, Kota S. Synthesis of multistable equilibrium compliant mechanisms using combinations of bistable mechanisms. Journal of Mechanical Design, Transactions of the ASME 2009;131(2):0210021–02100211. doi:10.1115/1.3013316.
[18] Pham HT, Wang DA. A quadristable compliant mechanism with a bistable structure embedded in a surrounding beam structure. Sensors and Actuators, A: Physical 2011;167(2):438–48. doi:10.1016/j.sna.2011.02.044.
[19] Kay ABM, Smith DG, Magleby SP, Jensen BD, Howell LL. Metrics for evaluation and design of large-displacement linear-motion compliant mechanisms. Journal of Mechanical Design, Transactions of the ASME 2012;134(1):1–9. doi:10.1115/1.4004191.
[20] Rommers J, Naves M, Brouwer DM, Herder JL. A large range spatial linear guide with torsion reinforcement structures. ASME International 2018. doi:10.1115/detc2018-86424.
[21] Machekposhti D.F., Tolou N., Herder J.L.. A review on compliant joints and rigid-body constant velocity universal joints toward the design of compliant homokinetic couplings. 2015. DOI: 10.1115/1.4029318.
[22] Wiersma DH, Boer SE, Aarts RG, Brouwer DM. Design and performance optimization of large stroke spatial flexures. J Comput Nonlinear Dyn 2014;9(1). doi:10.1115/1.4025669.
[23] Trease BP, Moon Y-M, Kota S. Design of large-displacement compliant joints. J Mech Des 2004;127(4):788–98. doi:10.1115/1.1900149.
[24] Henein S, Spanoudakis P, Droz S, Myklebust LI, Onillon E. Flexure pivot for aerospace mechanisms. In: Proceedings of the 10th ESMATS/ ESA, San Sebastian, San Sebastian; 2003. Pp. Paper No. ESA SP–524
[25] Fowler RM, Maselli A, Pluimers P, Magleby SP, Howell LL. Flex-16: large-displacement monolithic compliant rotational hinge. Mech Mach Theory 2014;82:203–17. doi:10.1016/j.mechmachtheory.2014.08.008.
[26] Howell LL. Compliant mechanisms. New York,US: John Wiley and Sons Inc; 2001.
[27] Paros J, Weisbord L. How to design flexure hinges. Machine Design 1965;25:151–6.
[28] Linß S, Milojević A, Pavlović N, Zentner L. Synthesis of compliant mechanisms based on goal-oriented design guidelines for prismatic flexure hinges with polynomial contours. In: 2015 IFToMM world congress proceedings, IFToMM 2015; 2015. DOI: 10.6567/IFToMM.14TH.WC.PS10.008.
[29] Linß S, Schorr P, Zentner L. General design equations for the rotational stiffness, maximal angular deflection and rotational precision of various notch flexure hinges. Mech Sci 2017;8(1):29–49. doi:10.5194/ms-8-29-2017.
[30] Haringx JA. The cross-spring pivot as a constructional element. Appl Sci Res 1949;1(1):313–32. doi:10.1007/BF02120338.
[31] Olson JL. Evalution of flexural pivots to meet critical performance and life requirements. Design News, Vol. 25, p. 139.. Oak Brook, IL: Cahners-Denver Publishing CO; 1970.
[32] Jensen BD, Howell LL. The modeling of cross-axis flexural pivots. Mech Mach Theory 2002;37(5):461–76. doi:10.1016/S0094-114X(02)00007-1.
[33] Zelenika S, De Bona F. Analytical and experimental characterisation of high-precision flexural pivots subjected to lateral loads. Precis Eng 2002;26(4):381–8. doi:10.1016/S0141-6359(02)00149-6.
[34] Morsch FM, Herder JL. Design of a generic zero stiffness compliant joint. In: Proceedings of the ASME design engineering technical conference, Vol. 2; 2010. p. 427–35. DOI: 10.1115/DETC2010-28351
[35] Merriam EG, Howell LL. Lattice flexures: geometries for stiffness reduction of blade flexures. Precis Eng 2016;45:160–7. doi:10.1016/j.precisioneng.2016.02.007.
[36] Garcia Rodriquez L. Development of a fully flexure-based prosthetic hand, The Netherlands: University of Twente, Enschede; 2018. Ph.d. thesis. DOI: 10.3990/1.9789036545808
[37] Pei X, Yu J, Zong G, Bi S, Hu Y. A novel family of leaf-type compliant joints: combination of two isosceles-trapezoidal flexural pivots. J Mech Robot 2009;1(2):1–6. doi:10.1115/1.3046140.
[38] Fowler RM, Maselli A, Pluimers P, Magleby SP, Howell LL. Flex-16: a large-displacement monolithic compliant rotational hinge. Mech Mach Theory 2014;82:203–17. doi:10.1016/j.mechmachtheory.2014.08.008.
[39] Zhang J, Guo H-W, Zhang ZN. Design of flexure revolute joint based on double compliant curved beam. Proceedings of the Institution of Mechanical Engineers, Part C: Journal of Mechanical Engineering Science 2019;233(13):4521–30. doi:10.1177/0954406219833085.
[40] Cannon JR, Howell LL. A compliant contact-aided revolute joint. Mech Mach Theory 2005;40(11):1273–93. doi:10.1016/j.mechmachtheory.2005.01.011.
[41] Goldfarb M, Speich JE. A well-behaved revolute flexure joint for compliant mechanism design. J Mech Des 1999;121(3):424–9. doi:10.1115/1.2829478.
[42] Herder JL, van den Berg FPA. Statically balanced compliant mechanisms (SBCM's), an example and prospects. In: Proceedings of the ASME 2000 international design engineering technical conferences and computers and information in engineering conference. Volume 7B: 26th biennial mechanisms and robotics conference. Baltimore, Maryland, USA. September 10–13, pp., 2000., DOI: DETC2000/MECH-14144; 2000.

[43] Schenk M, Guest SD. On zero stiffness. Proceedings of the Institution of Mechanical Engineers, Part C: Journal of Mechanical Engineering Science 2014;228(10):1701–14. doi:10.1177/0954406213511903.
[44] Cannon JR. Compliant mechanisms to perform bearing and spring functions in high precision applications. Brigham Young University; 2004. Msc thesis.
[45] Zhao H, Zhao C, Ren S, Bi S. Analysis and evaluation of a near-zero stiffness rotational flexural pivot. Mech Mach Theory 2019;135:115–29. doi:10.1016/j.mechmachtheory.2019.02.003.
[46] Merriam EG, Howell LL. Non-dimensional approach for static balancing of rotational flexures. Mech Mach Theory 2015;84:90–8. doi:10.1016/j.mechmachtheory.2014.10.006.
[47] Bilancia P, Smith SP, Berselli G, Magleby SP, Howell LL. Zero torque compliant mechanisms employing pre-buckled beams. J Mech Des 2020:1–14. doi:10.1115/1.4046810.
[48] Hou CW, Lan CC. Functional joint mechanisms with constant-torque outputs. Mech Mach Theory 2013;62:166–81. doi:10.1016/j.mechmachtheory.2012.12.002.
[49] Prakashah HN, Zhou H. Synthesis of constant torque compliant mechanisms. J Mech Robot 2016;8(6). doi:10.1115/1.4034885.
[50] Lachenal X, Daynes S, Weaver PM. A non-linear stiffness composite twisting i-beam. J Intell Mater Syst Struct 2014;25(6):744–54. doi:10.1177/1045389X13502853.
[51] Li J, Fu K, Gu Y, Zhao Z. Torsional negative stiffness mechanism by thin strips. Theor Appl Mech Lett 2019;9(3):206–11. doi:10.1016/j.taml.2019.01.012.
[52] Calladine CR. Theory of shell structures. Cambridge: Cambridge University Press; 1983. doi:101017/CBO9780511624278.